Chinese Chemical Letters 33 (2022) 2721–2725

Contents lists available at ScienceDirect

Chinese Chemical Letters

journal homepage: www.elsevier.com/locate/cclet

Adsorption of aqueous Cu(II) and Ag(I) by silica anchored Schiff base decorated polyamidoamine dendrimers: Behavior and mechanism

Kaiyan Wu, Bingxiang Wang, Bentian Tang, Liping Luan, Wenlong Xu, Beibei Zhang, Yuzhong Niu*

School of Chemistry and Materials Science, Ludong University, Yantai 264025, China

ARTICLE INFO

Article history:
Received 14 July 2021
Revised 9 August 2021
Accepted 30 August 2021
Available online 6 September 2021

Keywords:
Silica
PAMAM dendrimers
Adsorption mechanism
Theoretical calculation

ABSTRACT

A class of silica anchored Schiff base decorated polyamidoamine (PAMAM) dendrimers were synthesized for removing aqueous Cu(II) and Ag(I). The adsorption performance was investigated synthetically and the adsorption mechanism was revealed. Results indicate the adsorption capacity depends on dendrimer generation, solution pH, contact time, temperature and initial metal ion concentration. The optimum adsorption pH is 6 for both metal ion. Adsorption kinetic suggests the adsorption can achieve equilibrium at 180 and 150 min for Cu(II) and Ag(I). The kinetic process is found to be in good agreement with *pseudo*-second-order model and film diffusion is the rate-controlling step. The adsorption isotherm indicates the adsorption is proceeded by monolayer behavior with chemical mechanism. These adsorbents exhibit competitive adsorption capacity as compared with other reported adsorbents. Theoretical calculation demonstrates the participation of hydroxyl, carbonyl, and amide groups during the adsorption of Cu(II), while hydroxyl and amide groups are mainly responsible for capturing Ag(I).

Water pollution caused by the discharge of metal ions has posed a great threat to human health and the ecological system [1–3]. The metal ions are non-biodegradable and high toxic, which can be accumulated in food chain and leading to the deactivation of protein [4,5]. Cu(II) and Ag(I) are two common ions that generally discharged from alloy manufacture, electroplating, antifouling paints, and steel production fields [6,7]. The intake of excess Cu(II) can cause liver damage and body function disorders, while excess Ag(I) can cause the diseases of skin pigmentation, liver and kidney degeneration, and respiratory disorders [7,8]. Therefore, the seeking of ideal method for the remediation of Cu(II) and Ag(I) pollution is still a hot topic.

Different techniques involve membrane separation, ion exchange, solvent extraction, chemical precipitation, and adsorption have been utilized for removing heavy metal ions [9–11]. The excellent properties of high efficiency, easy operation and cost-effectiveness of adsorption method make it widely used for the decontamination of metal ions [12,13]. Multifarious functional groups have been employed for the construction of adsorbents to remove Cu(II) and Ag(I) from an aqueous solution. For example, Fronczak *et al.* synthesized amino functionalized graphitic carbon nitride to adsorb Cu(II) [14]. Guibal *et al.* employed 2-mercaptobenzimidazole derivative to modify chitosan for the adsorption and recovery of Ag(I) [15]. Yuan *et al.* prepared polypyrrole–Mo_3S_{13} by incorporating nitrogen and sulfur to realize the adsorption of Ag(I) and Cu(II) [16].

Polyamidoamine (PAMAM) dendrimer displays outstanding metal ion binding ability due to the existence of high density of nitrogen and oxygen atoms and numerous internal cavities [17,18]. Moreover, it can be decorated with various functional groups to enhance the adsorption performance for the targeted metal ion [19,20]. Hence, the fabrication of PAMAM dendrimer based adsorbents has attracted special attentions [20,21]. However, both PAMAM dendrimer and their metal ion chelates are generally solvated in aqueous solution, which hinders its application in metal ion separation. One of the promising methods to overcome this defect is to immobilize PAMAM dendrimer onto the solid substrates such as cellulose, magnetic Fe_3O_4, silica [21,22]. For instance, Wang *et al.* constructed PAMAM dendrimer modified nanocrystalline cellulose and used it for the adsorption of Cu(II) [21]. Cheng *et al.* prepared PAMAM dendrimer decorated magnetic halloysite nanotubes for efficient removing Pb(II) [22]. Our group also constructed several PAMAM dendrimers based adsorbents by decorating silica and magnetic Fe_3O_4 to realized the selective adsorption of

* Corresponding author.
E-mail address: niuyuzhong@ldu.edu.cn (Y. Niu).

https://doi.org/10.1016/j.cclet.2021.08.126
1001-8417/

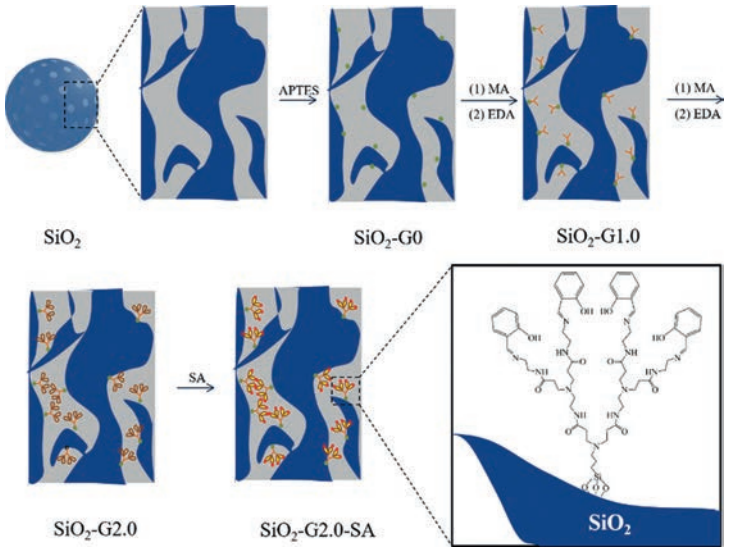

Scheme 1. The ideal synthetic route of SiO_2-G2.0-SA.

Hg(II) [20,23]. Among these substrates, silica is widely used due to the merits of large surface area, easy functionalization, excellent thermal and chemical stability, and high porosity [23]. Previous research demonstrated that the adsorption performance of these adsorbents greatly depends on the peripheral groups of PAMAM dendrimer [20]. Schiff base represents a set of functional groups that formed by the reaction of amine and aldehyde groups, and exhibits high affinity for metal ions [24–26]. Thus, the import of Schiff base functional group to the peripheral of PAMAM dendrimers is assumed to construct adsorbents with marked binding ability, and realized the efficient adsorption of Cu(II) and Ag(I) from aqueous solution.

In the present study, a class of silica anchored Schiff base decorated polyamidoamine dendrimers (SiO_2-G0-SA, SiO_2-G1.0-SA and SiO_2-G2.0-SA) was prepared. The as-prepared adsorbents were utilized for the adsorption of Cu(II) and Ag(I). The adsorption behavior was investigated systematically and the adsorption mechanism was demonstrated by density functional method (DFT) calculation.

SiO_2-G0-SA, SiO_2-G1.0-SA and SiO_2-G2.0-SA were prepared via the method described in our previous research, and the synthetic route was illustrated in Scheme 1 by selecting SiO_2-G2.0-SA as representative [23]. The brief description of the reagents and methods were described in Supporting information.

The saturated adsorption amount was detected by the following procedures: About 20 mg adsorbents and 20 mL of 0.005 mol/L Cu(II) or Ag(I) solution were charged into the flask and shaken at 25 °C for 12 h. Then, the residual metal ion after adsorption was detected by atomic absorption spectrophotometer (AAS). The adsorption capacity was obtained by Eq. S1 (Supporting information). The impact of solution pH, temperature, initial concentration, and time on the adsorption, as well as the theoretical calculation on the adsorption mechanism were evaluated by similar procedures reported previously [27]. The specific description of the procedures was exhibited in the supporting information.

The adsorption capacity of the adsorbents for the two ions is depicted in Fig. S1 (Supporting information). The adsorption capacity for Cu(II) increases in the order of SiO_2-G0-SA < SiO_2-G1.0-SA < SiO_2-G2.0-SA, while that for Ag(I) follows the order of SiO_2-G0-SA < SiO_2-G2.0-SA < SiO_2-G1.0-SA. Theoretically, the number of binding sites would increase with the dendrimer generation increase. Hence, the adsorption capacity of the adsorbents for Cu(II) increases accordingly. However, the trend for Ag(I) is different and SiO_2-G1.0-SA exhibits the largest adsorption amount. The probable reason for the decrease of adsorption capacity of SiO_2-G2.0-SA is mainly due to the presence of intermolecular or intramolecular crosslinking structure in PAMAM dendrimer that formed during the synthesis process, which blocked the binding of metal ions to the interior functional groups of PAMAM dendrimer [28]. Compared with Cu(II), the ionic radius of Ag(I) is larger, which indicates the crosslinking structure has a greater impact. Thus, the adsorption capacity of SiO_2-G2.0-SA is decreased.

The effect of solution pH on the adsorption of Cu(II) and Ag(I) by the adsorbents was detected in the range of 1-6, and the result is shown in Fig. S2 (Supporting information). The obtained result reveals the dependency of adsorption capacity on solution pH. The adsorption amount is observed to be increased as the pH value changes from 1 to 6. The trend can be assigned to the presence of superabundant H^+ at low pH, and H^+ prefers to compete for the active binding sites with metal ions, leading to the chelation between metal ions and the adsorbent became weak [28]. Furthermore, the excessive H^+ can promote the protonation of functional groups of –NH–, –N= and OH. The electrostatic repulsion between metal ion and functional group prevents the metal ions from touching with the adsorbent [29,30]. More binding sites are suitable for binding of metal ion due to the deprotonation of functional groups with the increase of solution pH. Hence, the adsorption amount increases accordingly with the increase of pH. As the solution pH increases over 6, the precipitation of Cu(II) and Ag(I) would appear and causes the metal adsorption studies inaccurate. Similar phenomena were also observed for the adsorption of Cu(II) and Ag(I) by calcined fly ash and thioether/carboxyl-functionalized polymers in previous reports [31,32]. Hence, the optimum pH 6 was selected for the following adsorption experiments.

The adsorption kinetics for Cu(II) and Ag(I) are presented in Fig. 1. The adsorption proceeds fast in the first 70 min. Take SiO_2-G2.0-SA as example, the adsorption amount are 0.18 and 0.32 mmol/g for Cu(II) and Ag(I) at 70 min, which accounts for 57.39% and 81.73% of the equilibrium adsorption capacity. And then, the adsorption proceeds progressively until reaching equilibrium at 180 and 150 min for Cu(II) and Ag(I). The equilibrium adsorption capacity are 0.48 and 0.39 mmol/g for Cu(II) and Ag(I), respectively. The fast adsorption at the initial is attributed to the presence of large number of available active binding sites and high concentration of metal ions, which facilitates the contact and interaction

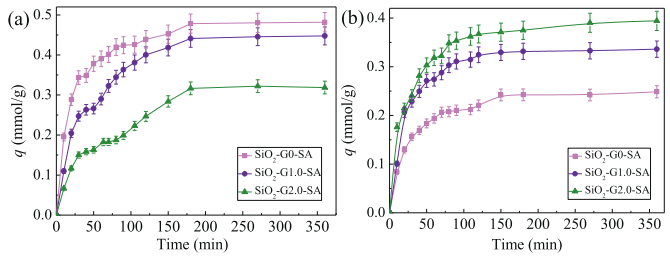

Fig. 1. The adsorption kinetic curves of Cu(II) (a) and Ag(I) (b) (T = 25 °C, pH 6, $m_{adsorbents}$ = 20 mg, $C_{Cu(II)}$ = 0.005 mol/L, $C_{Ag(I)}$ = 0.005 mol/L).

between them [33]. With the contact time extended, the adsorption rate gradually turns slow until reach equilibrium after a quick occupation of available binding sites by Cu(II) and Ag(I).

Pseudo-first-order (PFO) model, pseudo-second-order (PSO) model, and Boyed film diffusion (BFD) model were utilized to explore the kinetic mechanism and are described in the supporting information [34,35]. The fitting parameters were presented in Tables S1 and S2 (Supporting information). It can be deduced from Table S1 that PSO shows better fitting for the adsorption kinetic data as the correlation coefficients ($R_2{}^2$) of PSO are all higher than those of PFO ($R_1{}^2$). Besides, the adsorption capacity ($q_{e,cal}$) calculated from PSO are consist with the experimental result ($q_{e,exp}$), further confirms the fitness of PSO. The plots of B_t (the mathematical function of fractional attainment of equilibrium) *versus* t in Table S2 are found to exhibit linear behavior and do not pass through the origin, suggesting film diffusion dominates the kinetic process [27].

Fig. 2 shows the adsorption isotherms of the two ions at different temperatures. The adsorption was promoted by increasing temperature and initial metal ion concentration. Take SiO_2-G2.0-SA for example, the adsorption amount for Cu(II) increases from 0.32 to 0.48 mmol/g when the initial Cu(II) concentration increases from 0.001 to 0.005 mol/L under 35 °C. The promotion of the adsorption by raising concentration is ascribed to the increasing driving force under high concentration that promotes the transfer of metal ion to the adsorbent [36]. As for the influence of temperature, the adsorption amount for Cu(II) is increased from 0.06 mmol/g to 0.32 mmol/g with the temperature varies from 15 °C to 35 °C under the concentration of 0.001 mol/L. The result suggests that the adsorption was conducted endothermically [37].

The isotherms data were analyzed by Freundlich, Langmuir, and Dudinin-Radushkevich (D-R) models [38–40]. The description of these models is given in the supporting information, and the fitting results are summarized in Tables S3 and S4 (Supporting information). By comparison of the fitting results in Table S3, Langmuir model is found to fit better according to the higher correlation coefficient ($R_L{}^2$). Hence, the adsorption can be assigned to monolayer adsorption [41]. Moreover, the mean free energy (E, kJ/mol) calculated from D-R model in Table S4 falls in the range of 8-16 kJ/mol, suggesting the uptake of Cu(II) and Ag(I) by the adsorbents is proceeded in chemical nature [38].

The comparison of the maximum adsorption capacity (q_m) with other adsorbents is listed in Table S5 (Supporting information) [42–55]. It is apparent that the as-prepared adsorbents exhibit competitive adsorption capacity as compared with other adsorbents, suggesting they can be potentially used for the separation and preconcentration of aqueous Cu(II) and Ag(I).

Adsorption selectivity of the adsorbents was determined by selecting SiO_2-G2.0-SA for Cu(II) as a representative, and the result is recorded in Table S6 (Supporting information). It can be seen SiO_2-G2.0-SA exhibits good adsorption selectivity for Cu(II) in the binary metal ion systems with the presence of coexisting metal ions of Cd(II), Mn(II), Ni(II), Zn(II) and Co(II). Especially in the systems of Cu(II)-Cd (II), Cu(II)-Mn(II) and Cu(II)-Ni(II), SiO_2-G2.0-SA can 100% selective adsorption of Cu(II). The good adsorption selectivity for Cu(II) can be explained by Hard-Soft Acid-Base (HSAB) theory. The nitrogen atom of Schiff base functional group attributes to soft base and exhibits good binding ability toward Cu(II) that belongs to soft acid [56]. Although Cd(II) also belongs to soft acid, its acidity is lower than Cu(II). Hence, the adsorption capacity for Cu(II) is superior to Cd(II). Compared with Cu(II), Mn(II), Ni(II), Zn(II) and Co(II) are all attributed to borderline acid [56]. Thus, the binding ability for these metal ions is weaker than Cu(II), leading to the good adsorption selectivity for Cu(II) in the presence of these metal ions.

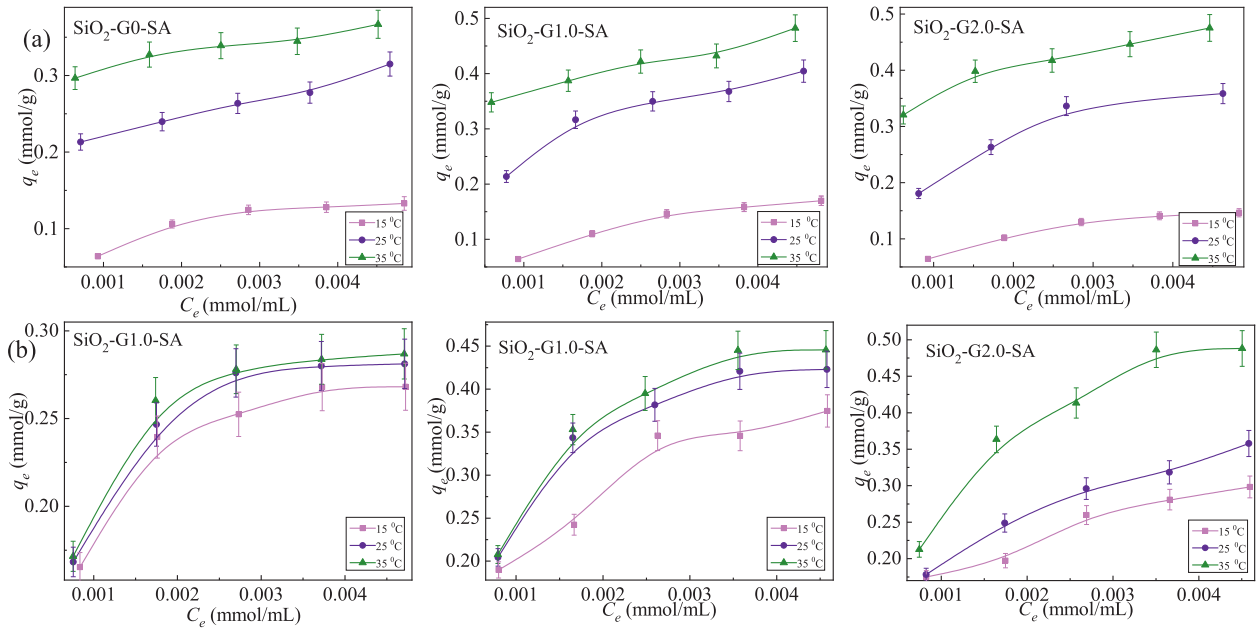

Fig. 2. Adsorption isotherms behavior for Cu(II) (a) and Ag(I) (b) (T = 15-35 °C, pH 6, $m_{adsorbents}$ = 20 mg, $C_{Cu(II) \text{ or } Ag(I)}$ = 0.001-0.005 mol/L).

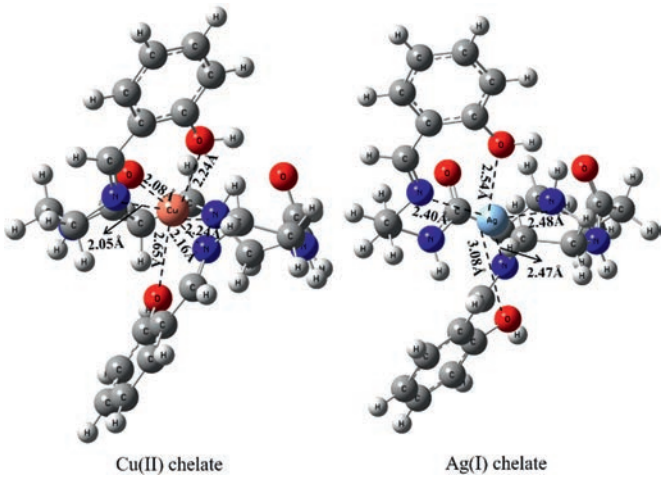

Fig. 3. The optimized configuration of Cu(II) and Ag(I) chelate.

The adsorption mechanism was revealed by density functional theory (DFT) calculation by using Gaussian 03 suits of program. The branching unit of G2.0-SA is chosen as computational model to interact with metal ions because of the symmetric structure of the dendrimer. The optimized configurations of the chelates that formed by metal ions and computational model are expressed in Fig. 3. The computational model interacts with Cu(II) by the oxygen atoms of hydroxyl (O1 and O2) and carbonyl (O3) groups, nitrogen atoms of imino (N1 and N2) and tertiary amine (N3) groups to form stable hexa-coordinated chelates, while it tends bind Ag(I) with O1, O2, N1, N2, and N3 to form penta-coordinated chelates. For Cu(II) chelate, the O-Cu bonds length that formed with O1 and O2 are 2.24 and 2.65 Å, whereas that of O3 is 2.08 Å, the difference in the bond length suggests the interaction between O3 and Cu(II) is stronger than that of O1 and O2. Similarly, the N1-Cu and N2-Cu bonds are 2.16 and 2.05 Å in length, while that of N3-Cu is 2.24 Å, indicating Cu(II) is preferred to be bonded by N1 and N2 as compared with N3. For Ag(I) chelate, the bonds of O-Ag are 2.54 and 3.08 Å in length, while N1-Ag, N2-Ag, and N3-Ag bonds are 2.40, 2.47, and 2.48 Å in length, respectively. The binding energy for the two chelates is −403.48 and −615.60 kcal/mol, suggesting the adsorbent prefers to bind Ag(I) than Cu(II), which is consistent with the result of adsorption capacity as SiO_2-G2.0-SA exhibits better adsorption performance for Ag(I).

The FTIR spectra of the adsorbents before and after adsorption were measured by selecting SiO_2-G2.0-SA as a representative to interpret the adsorption mechanism, and the results are shown in Fig. S2a (Supporting information). For SiO_2-G2.0-SA, the wide absorption peak at about 3286 cm^{-1} is attributed to the stretching vibration of N–H and O–H groups. The absorption peaks at 1639 and 1545 cm^{-1} are attributed to the stretching vibration of C=O and bending vibration of N-H groups. Moreover, the absorption peak of aromatic rings of salicylic can be observed at about 1453 cm^{-1}. After adsorption, the absorption peaks of the stretching and bending vibration of N-H groups, as well as C=O groups are all become smaller in the spectra of SiO_2-G2.0-SA-Cu(II) and SiO_2-G2.0-SA-Ag(I), suggesting the participation of C=O and N-H groups during the adsorption. As a comparison, the calculated FTIR spectra of the computational model and the chelates are also provided in Fig. S2b (Supporting information). The computational model exhibits the characteristic absorption peaks of hydroxyl, carbonyl and N-H of amide groups at 3208, 1730 and 1561 cm^{-1}, respectively. After chelating with Cu(II), the peaks of hydroxyl and amide groups become weaker and that of carbonyl groups are disappeared, suggesting the participation of hydroxyl, carbonyl, and amide groups during the adsorption of Cu(II). Similarly, the absorption peaks of hydroxyl and amide groups also become weaker after coordinating with Ag(I), implying the contribution of hydroxyl and amide groups to the adsorption of Ag(I). However, there is no obvious change for the absorption peak of carbonyl groups, which indicates the carbonyl groups are not taking part in the chelation. The above results are consistent with the results of configuration analysis of the optimized chelate.

Natural bond orbital (NBO) analysis is used to further clarify the adsorption mechanism [36,57]. Bond order obtained from NBO analysis is important for estimating the interaction of the chelate [58]. Table S7 (Supporting information) summarizes the bond orders of the coordinate bond in the chelates. The bond order of O1-Cu and O2-Cu are smaller than O3-Cu by 0.0686 and 0.0464, further demonstrating the binding ability of O3 in the adsorbent is superior than that of O1 and O2 for Cu(II). As for N-Cu coordinate bonds, the bond orders of N1-Cu and N2-Cu are higher than N3-Cu by 0.0125 and 0.0168, suggesting the interaction between N1, N2 and Cu(II) is stronger than that of N3. A similar result can be also observed for Ag(I) chelate, as the bond orders of N1-Ag and N2-Ag are higher than N3-Ag by 0.0017 and 0.0075, respectively.

The charge of Cu(II) and Ag(I) in the chelates are 1.36 and 0.82, which are smaller than the charge of free Cu(II) and Ag(I), suggesting charge transfer from computational model to metal ions take place during the chelation. The electronic configurations of Cu(II) and Ag(I) are $4s^{0.26}3d^{9.37}4p^{0.01}$ and $5s^{0.20}4d^{9.95}6s^{0.01}6p^{0.01}$, indicating the transferred charge mainly distributes on 4s and 5s orbital of Cu(II) and Ag(I). The profiles of the highest occupied molecular orbital (HOMO) and lowest unoccupied orbital (LUMO) are illustrated in Fig. S3 (Supporting information). The HOMO of the computational model is dominantly located on the tertiary amine N, carbonyl O, and the C atoms in the middle of them. After chelating with Cu(II) and Ag(I), the HOMO is mainly presented on the phenyl ring and its adjacent hydroxyl O and imino N atoms, as well as Cu(II) and Ag(I) atoms, further suggesting the charge transfer from computational model to metal ion during the chelation. The LUMO of the computational model presents the charge location on the phenyl ring and its neighbor hydroxyl O and imino N atoms. However, the LUMO of Cu(II) and Ag(I) chelate is mainly spread over on the hydroxyl O atom, phenyl ring, imino N atom, and C atom between them.

The stabilization energy ($E(2)$) that obtained from second-order perturbation theory analysis is presented in Table S8 (Supporting information), and is used to further evaluate the charge transfer and interaction during the chelation. As can be seen from Table S8, the interaction between the computational model and metal ions is dominated by charge transfer from the lone pair of electrons of the functional group to the empty orbital of metal ions. For Cu(II) chelate, the σ donation of lone pair electrons of N and O to the empty orbital of Cu(II) (LP(N or O) → LP*(Cu)) governs the chelation. The $E(2)$ for LP(N) → LP*(Cu) are 9.26, 10.03, and 10.18 kcal/mol, and those of LP(O) → LP*(Cu) are 5.08, 3.18, and 4.20 kcal/mol. The $E(2)$ values of LP(N) → LP*(Cu) are higher than LP(O) → LP*(Cu), suggesting N1, N2 and N3 dominate the chelation. A similar trend can also be observed for Ag(I) chelate, as the $E(2)$ of LP(N) → LP*(Ag) are also higher than LP(O) → LP*(Ag).

In summary, SiO_2-G0-SA, SiO_2-G1.0-SA and SiO_2-G2.0-SA were synthesized for the adsorption of Cu(II) and Ag(I) from aqueous solution. The result implies the adsorption displays strong solution pH dependence and the optimum adsorption pH is 6. The adsorption can achieve equilibrium at about 180 and 150 min for Cu(II) and for Ag(I), respectively. Adsorption kinetic is found to be in good agreement with PSO model and film diffusion is the rate-controlling step. Adsorption isotherm shows the adsorption increase with the increase of temperature and initial metal con-

centration. The adsorption is regarded to be proceeded by monolayer behavior with chemical mechanism. The comparison of q_m with other adsorbents indicates the as-prepared adsorbents exhibit a relatively higher adsorption capacity. The adsorption mechanism is further revealed based on DFT calculation and FTIR analysis. Results demonstrate that the hydroxyl, carbonyl, and amide groups participate in the capture Cu(II), while hydroxyl and amide groups are mainly responsible for the uptake of Ag(I).

Declaration of competing interest

The authors declare that they have no known competing financial interests or personal relationships that could have appeared to influence the work reported in this paper.

Acknowledgment

Natural Science Foundation of Shandong Province (No. ZR2018MB039) is acknowledged.

Supplementary materials

Supplementary material associated with this article can be found, in the online version, at doi:10.1016/j.cclet.2021.08.126.

References

[1] D. Dai, J. Yang, Y. Wang, et al., Adv. Funct. Mater. 31 (2021) 2006168.
[2] L. Wang, Q. Xiao, D. Zhang, et al., ACS Appl. Mater. Interfaces 12 (2020) 36652–36659.
[3] H. Jiang, W. Zhang, P. Chen, et al., J. Mater. Chem. A 4 (2016) 11897–11907.
[4] X. Zheng, H. Zheng, Z. Xiong, et al., Chem. Eng. J. 392 (2020) 123706.
[5] X. Song, Y. Niu, Z. Qiu, et al., Fuel 206 (2017) 80–88.
[6] A. Tomczyk, Z. Sokolowska, P. Boguta, Fuel 278 (2020) 118168.
[7] N. Li, Z. Li, L. Zhang, et al., J. Hazard. Mater. 382 (2020) 121113.
[8] S. Zhu, M. Khan, F. Wang, Z. Bano, M. Xia, Chem. Eng. J. 392 (2020) 123711.
[9] A. Li, H. Deng, Y. Jiang, et al., Langmuir 36 (2020) 9160–9174.
[10] M. Saifuddin, J. Bae, K. Kim, Water Res. 158 (2019) 246–256.
[11] G. Nie, S. Qiu, X. Wang, et al., Chin. Chem. Lett. 32 (2021) 2342–2346.
[12] Q. Zhang, S. Bolisetty, Y. Cao, et al., Angew. Chem. Int. Ed. 58 (2019) 6012–6016.
[13] M. Razanajatovo, W. Gao, Y. Song, et al., Chin. Chem. Lett. 32 (2021) 2637–2647.
[14] M. Fronczak, K. Demby, P. Strachowski, M. Strawski, M. Bystrzejewski, Langmuir 34 (2018) 7272–7283.
[15] K. Elwakeel, A. Al-Bogami, E. Guibal, Chem. Eng. J. 403 (2021) 126265.
[16] M. Yuan, H. Yao, L. Xie, et al., J. Am. Chem. Soc. 142 (2020) 1574–1583.
[17] Y. Lee, S. Zhang, K. Yu, J. Choi, W. Ahn, Chem. Eng. J. 378 (2019) 122133.
[18] N. He, H. Li, C. Cheng, X. Wang, et al., Chem. Eng. J. 395 (2020) 125162.
[19] M. Camarada, J. Comer, H. Poblete, et al., Langmuir 34 (2018) 10063–10072.
[20] Y. Zhou, L. Luan, B. Tang, et al., Chem. Eng. J. 398 (2020) 125651.
[21] Y. Wang, Q. Lu, Cellulose 27 (2019) 2173–2187.
[22] D. Cheng, X. Dai, L. Chen, et al., ACS Sustainable Chem. Eng. 8 (2019) 771–781.
[23] Y. Niu, R. Qu, H. Chen, et al., J. Hazard. Mater. 278 (2014) 267–278.
[24] W. Qiao, P. Zhang, L. Sun, et al., Chin. Chem. Lett. 31 (2020) 2742–2746.
[25] N. Senda, I. Fujiwara, Y. Murakami, Appl. Clay Sci. 183 (2019) 105310.
[26] J. Zhao, Y. Niu, B. Ren, et al., Chem. Eng. J. 347 (2018) 574–584.
[27] Z. Chen, B. Tang, Y. Niu, et al., Fuel 286 (2021) 119287.
[28] Y. Niu, R. Qu, C. Sun, et al., J. Hazard. Mater. 244 (2013) 276–286.
[29] C. Xiong, S. Wang, L. Zhang, et al., J. Mol. Liq. 254 (2018) 340–348.
[30] Z. Sutirman, M. Sanagi, K. Abd Karim, W. Ibrahim, B. Jume, Int. J. Biol. Macromol. 116 (2018) 255–263.
[31] C. Wang, J. Wang, S. Wang, R. Yang, H. Wang, Materials 13 (2020) 4621.
[32] Y. Huang, W. Zhao, X. Zhang, H. Peng, Y. Gong, Chem. Eng. J. 375 (2019) 121935.
[33] S. Ghodsi, M. Behbahani, M. Badi, et al., J. Mol. Liq. 323 (2021) 114472.
[34] Y. Ho, J. Hazard. Mater. 136 (2006) 681–689.
[35] G. Boyd, J. Schubert, A. Adamson, J. Am. Chem. Soc. 69 (1947) 2818–2829.
[36] L. Luan, B. Tang, Y. Liu, et al., Sep. Purif. Technol. 257 (2021) 117902.
[37] A. Kumar, H. Jena, J. Environ. Chem. Eng. 5 (2017) 2032–2041.
[38] J. Dron, A. Dodi, J. Hazard. Mater. 190 (2011) 300–307.
[39] X. Song, Y. Niu, P. Zhang, et al., Fuel 199 (2017) 91–101.
[40] Z. Zhang, Y. Niu, H. Chen, et al., ACS Sustain. Chem. Eng. 7 (2019) 7324–7337.
[41] M. Shafiee, R. Foroutan, K. Fouladi, et al., Adv. Powder Technol. 30 (2019) 544–554.
[42] J. Kang, H. Liu, Y. Zheng, J. Qu, J. Chen, J. Colloid Interface Sci. 344 (2010) 117–125.
[43] B. Abbar, A. Alem, S. Marcotte, et al., Process Saf. Environ. Prot. 109 (2017) 639–647.
[44] C. Jeon, J. Ind. Eng. Chem. 17 (2011) 321–324.
[45] Y. Yu, J. Shapter, R. Popelka-Filcoff, J. Bennett, A. Ellis, J. Hazard. Mater. 273 (2014) 174–182.
[46] W. Ngah, L. Teong, R. Toh, M. Hanafiah, Chem. Eng. J. 209 (2012) 46–53.
[47] J. Han, Z. Du, W. Zou, H. Li, C. Zhang, Chem. Eng. J. 262 (2015) 571–578.
[48] Z. Wang, D. Kong, N. Qiao, et al., Appl. Surf. Sci. 457 (2018) 981–990.
[49] P. Vassileva, T. Radoykova, A. Detcheva, et al., Int. J. Environ. Sci. Technol. 13 (2016) 1319–1328.
[50] H. Ghassabzadeh, A. Mohadespour, M. Torab-Mostaedi, et al., J. Hazard. Mater. 177 (2010) 950–955.
[51] S. Coruh, G. Senel, O. Ergun, J. Hazard. Mater. 180 (2010) 486–492.
[52] C. Jeon, J. Ind. Eng. Chem. 53 (2017) 261–267.
[53] W. Nitayaphat, T. Jintakosol, J. Clean. Prod. 87 (2015) 850–855.
[54] M. Cantuaria, A. Neto, E. Nascimento, M. Vieira, J. Clean. Prod. 112 (2016) 1112–1121.
[55] T. Yang, L. Zhang, L. Zhong, et al., Hydrometallurgy 175 (2018) 179–186.
[56] R. Parr, R. Pearson, J. Am. Chem. Soc. 105 (1983) 7512–7516.
[57] R. Mulliken, J. Chem. Phys. 23 (1955) 2338–2342.
[58] Z. Javdani, H. Salehi, P. Amiri, Appl. Surf. Sci. 527 (2020) 146941.